An Investigation of the Chemical States of Copper in Methanol Catalysts and Their Relevance to Activity Maintenance

E. J. Karwacki, Jr., M. R. Anewalt, and D. M. Brown

Air Products and Chemicals, Inc.
Box 538, Allentown, PA 18105

Summary

Information on the chemical states of a catalyst surface is obtainable by X-Ray Photoelectron Spectroscopy (XPS). Copper-zinc oxide catalysts from the DOE sponsored Liquid Phase Methanol (LPMeOH) project have been studied to ascertain the oxidation states of copper on fresh, reduced, and spent catalyst samples. Using the Auger parameter to differentiate valence levels it is shown that Cu^{+1} must be maintained on the surface for continued catalyst activity to methanol. Unusually strong shifts, due to matrix effects, in the $Cu2p_{3/2}$ binding energy for reduced/active catalysts indicate that Cu^{+1} is stabilized by incorporation within the ZnO lattice. Energy Dispersive X-Ray Spectrometry (EDS) and XPS show that while the bulk Cu/Zn ratio is maintained at a value near 2.1 the surface Cu/Zn ratio decreases in use to well below unity. The effects of metal and halogen poisoning have also been studied by the additions of iron (as iron carbonyl) and chlorine, and are observed to deactivate the catalyst by reduction of Cu^{+1} to Cu^{0}. These results suggest a relationship between the copper state needed to maintain activity and the reducing/oxidizing potential of the reactant gases.

Introduction

Determination of the active copper state in copper/zinc/alumina catalysts, used for methanol synthesis, has been of recent interest (1-5). Klier and coworkers, using optical spectroscopy, have presented evidence indicating Cu^{+1}, dissolved in the ZnO lattice(1,2), as the catalytically active state. X-Ray Photoelectron Spectroscopy (XPS) has been employed by Okamato et al.(3,4) to show that CuO-ZnO samples containing less than 10% copper, upon reduction, do exhibit weak Cu(LMM) x-ray induced Auger lines suggestive of the presence of Cu^{+1}. The Okamato studies, unfortunately, do not present supporting data regarding activity of the catalysts to methanol synthesis. Himelfarb et al.(5) have presented evidence, by X-Ray Diffraction (XRD), for the existence of an intermediate Cu^{+1} phase during reduction of copper-zinc oxide catalysts. Since XRD is a bulk sensitive technique the chemical state of the surface is, however, still in doubt.

In conjunction with the current DOE sponsored Liquid Phase Methanol Project (LPMeOH) we have undertaken studies of commercially available copper-zinc oxide catalysts which have demonstrated actual activity to methanol synthesis in both the gas and liquid phases. Here we present XPS results which confirm that Cu^{+1} is indeed the active state. Poisoning by metal and/or halogens has also been investigated by XPS and Energy Dispersive X-Ray Spectrometry (EDS). Deactivation apparently occurs via reduction of Cu^{+1} to Cu^{0}.

Because the chemical shifts observed in the XPS spectrum for copper are limited it is necessary to employ the Auger parameter to follow the three valence states Cu^{0}, Cu^{+1}, and Cu^{+2}. The Auger parameter (α), proposed by Wagner(6) and later modified by Gaarenstrom and Winograd(7) is defined as:

$$\alpha + h\nu = BE_p + KE_A = \alpha' \qquad 1)$$

where $h\nu$ is the photon energy, BE_p the binding energy of the photoelectron peak, and KE_A the kinetic energy of the x-ray induced Auger line which is also observed in the spectrum. The addition of $h\nu$ to α is defined as α', the modified parameter(7), and is independent of the excitation energy.

From Equation 1 a plot of α' vs the corrected BE_p can be generated. This plot or Auger map, as it is referred, enables one, through analyses of standards, to assign regions to a particular elemental oxidation state or chemical environment.

Experimental

A commercially available copper-zinc oxide catalyst, in powdered form (2-7μm), has been used in these studies. Gas phase and in situ liquid phase reductions were performed by suitable laboratory adaptation of the commercial gas phase technique. Catalysts from liquid phase studies were prepared for surface analysis by stripping the inert oil via a series of cyclohexane washings in a nitrogen filled glove box. Upon drying, the samples were transported to an argon filled glove box. The catalyst samples were applied to a piece of double-sided adhesive tape attached to a sample mount. The mounts were then sealed in a vessel for transportation to the spectrometer. Under vacuum the vessels were reopened and the mounts attached to the transfer rod assembly.

XPS has been performed on a Physical Electronics 560 spectrometer equipped to perform XPS, Scanning Auger Microscopy (SAM), Ion Scattering Spectroscopy (ISS), and Secondary Ion Mass Spectrometry (SIMS). Mg $K\alpha$ radiation (1253.6eV) at 15 keV and 20mA was used as the excitation source. Charge correction was performed by referencing to the $Zn2p_{3/2}$ line at 1021.7eV and C1s, for residual oil, at 284.7eV. Both lines were found to agree to within $\pm$ 0.2eV.

EDS was performed on an Amray 1000 Scanning Electron Microscope (SEM) equipped with a Kevex 7000 spectrometer. Quantitative analysis was accomplished using ZAF corrections.

Copper oxide standards were prepared in situ by mounting a cleaned and polished (to 1μm alumina) copper foil to a probe that could be heated and cooled. After repeated cycles of ion sputtering and annealing at 300°C, a clean surface was obtained as verified by Auger Electron Spectroscopy (AES) and XPS. A thin film of CuO was then produced on the surface by heating the foil to 250°C under a stream of air. Larson(8) has reported that Cu_2O can be produced by reheating the CuO surface film to 250°C in vacuum. The advantage of this preparation is that surface charging is negligible due to the conduction of the thin oxide films produced on the surface.

Results and Discussion

Because of discrepancies in the literature(6,8), regarding the binding energy of the $Cu2p_{3/2}$ line, a study to determine α' for Cu, Cu_2O, and CuO was undertaken. The results of this investigation are listed in Table 1. The $Cu2p_{3/2}$ line is not observed to shift as copper metal is oxidized to Cu_2O, however, the Cu(LMM) line is found to move from 334.8eV to 336.8eV. This change causes a shift in α' from 1850.9eV, for copper metal, to 1848.9eV for Cu_2O. Further oxidation to CuO results in the $Cu2p_{3/2}$ line shifting to 933.2eV as well as the Cu(LMM) line to 335.6eV. The net result is a reshifting of α' back to 1851.2eV. These movements in α' are better illustrated by the Auger map, shown in Figure 1, which indicates the regions occupied by copper metal and its oxides. Though CuO and Cu metal possess the same α' value, the shift in the $Cu2p_{3/2}$ line, as well as the observation of satellites due to the paramagnetic nature of Cu^{+2} in the Cu2p spectrum, permits these chemical states to be distinguished.

The fresh, as received catalyst is found to be comprised of copper primarily as CuO. This is indicated by the observation of strong satellite peaks and an α' of 1851.0eV. Upon reduction, the Cu2p spectrum is observed to undergo a loss in satellite structure and a shift in the $Cu2p_{3/2}$ binding energy. Also, as shown in Table 1, the $Cu2p_{3/2}$ line is found to move from 933.6eV to 931.7eV. The x-ray induced Auger line, however, remains at 336.2eV. Calculating α' shows that the Cu^{+2} has been reduced to Cu^{+1}. To better illustrate these observed changes the Auger map is depicted in Figure 2. The region occupied by the reduced catalyst is in good agreement with the coordinates for Cu_2O in Figure 1. Thus it appears that Cu^{+1} is present on the surface after reduction. The binding energy shift observed for the $Cu2p_{3/2}$ line as the copper is reduced is observed to be significantly greater than expected for Cu^{+2} being reduced to the Cu^{+1} state. For Cu_2O, the $Cu2p_{3/2}$ line is found to be at 932.1eV while for the reduced sample a shift to 931.7eV is observed. This larger than anticipated chemical shift is believed to be attributable to matrix effects, similar to those observed by Kim and Winograd for Au implanted in SiO_2(9). The Cu^{+1} is apparently stabilized on the surface by its incorporation within ZnO lattice defects.(2) The electron rich environment offered by these sites is thus believed responsible for the large shift in the $Cu2p_{3/2}$ binding energy. In as received form (oxide), elemental analysis shows a Cu/Zn ratio of approximately 2 to 1. XPS measurements, however, clearly and reproducibly show a surface Cu/Zn ratio of almost unity.

After reduction the catalysts are used to produce methanol in either gas or liquid phase operations. Upon demonstration of satisfactory activity, samples of the catalysts are removed for analysis. In Table 1 and Figure 2 the results of studies on these active catalysts are also shown. The copper present on the surface is observed to exist as Cu^{+1} by the fact that α' remains at 1849.0eV. The surface Cu/Zn ratio, calculated by XPS, is found to decrease to approximately 0.7 to 1 upon reduction. This ratio becomes even smaller (0.3 - 0.1) after use in the reactor.

Upon an observed loss in activity a catalyst sample was again removed for analysis. The data, shown in Table 1 and Figure 2, indicates that Cu^{+1} has been reduced to Cu^0 by the observation of a shift in α' to 1851.0eV. It is our contention that deactivation is occurring by the reduction of Cu^{+1} to Cu^0 on the surface. this suggests that the continued presence of Cu^{+1} is important in maintaining catalytic activity.

The small particle size (2-7μm) of the catalyst powder used in liquid phase operations has permitted the use of EDS to rapidly determine a bulk Cu/Zn ratio for comparison with the surface ratio obtained by XPS. The results indicate that while the bulk Cu/Zn ratio remains at 2.1, a decrease in the surface Cu/Zn ratio, calculated by XPS, is observed upon reduction and use. Catalyst reduction decreases the surface Cu/Zn ratio from 1.0 to ~0.7. After use in methanol synthesis this ratio is found to further decrease to values approaching 0.3. This data fits well with proposals by Klier and coworkers(2) regarding specific site stabilization of Cu^{+1}. Since only a finite number of defect sites are anticipated within the ZnO lattice near the surface the Cu/Zn ratio is expected to decrease as Cu^{+1} dissolves within the ZnO lattice. Therefore recrystallization, due to excessive heat, is expected to severely effect the surface's ability to synthesize methanol. A requirement, for tight temperature control, thus is necessary to prevent surface recrystallization which suggests that the LPMeOH process offers significant advantages, as a result more efficient heat transfer, over gas phase synthesis.

Poisoning and its effects upon surface copper have also been investigated. The injection of a very low level of $Fe(CO)_5$ to the feed stream is observed to cause

a rapid deactivation of the catalyst. XPS indicates that no iron is apparently present on the surface of these samples. EDS analysis, however, shows that iron is present in the bulk of the poisoned samples. By XPS changes in the Cu(LMM) spectrum are observed. In Figure 3, the Cu(LMM) spectra for a fresh-reduced catalyst is compared with that obtained after iron poisoning. The observation of a second peak near 334.6eV is attributed to the presence of Cu^0 on the surface. Using Equation 1, α' is found to be equal to 1851.0eV for this new line. This region has been earlier determined, in the oxide study, to be occupied by metallic copper (Fig. 1). Thus upon contact with iron the Cu^{+1} is reduced to Cu^0, thereby deactivating the catalyst. Chlorine poisoning has also been investigated and the chlorine, likewise, appears to deactivate by reducing the surface Cu^{+1} to Cu^0. Unlike iron poisoning, XPS and EDS are both able to detect the presence of chlorine on the surface as well as a reduction in the Cu/Zn ratio at the catalyst surface. The mechanisms of deactivation are not well understood at this time and are currently the subject of continued research.

Conclusion

From this study it has been determined, using the Auger parameter, that Cu^{+1} is the active chemical state of copper on the surface, and is apparently stabilized by its incorporation within the ZnO lattice. Deactivation is believed to occur by the reduction of Cu^{+1} to Cu^0. Poisoning by either Fe or Cl is observed to also proceed through a mechanism by which the Cu^{+1} is reduced to Cu^0.

References

1. K. Klier, Adv. in Catalysis, 31, 243 (1982).

2. R. G. Herman, K. Klier, G. W. Simmons, B. P. Finn, and J. B. Bulko, J. of Catalysis, 56, 407 (1979).

3. Y. Okamąto, K. Fukino, T. Imanaku, and S. Teranishi, J. Chem. Soc., Chem. Commun., 1405 (1982).

4. Y. Okamato, K. Fukino, T. Imanaku, and S. Teranishi, J. Phys. Chem., 87, 3747 (1983).

5. P. B. Himelfarb, F. E. Wawner, Jr., A. Bieser, Jr., and S. N. Vines, J. of Catalysis, 83, 469 (1983).

6. C. D. Wagner, L. H. Gale, and R. H. Raymond, Anal. Chem., 51, 466 (1979).

7. S. W. Gaarenstrom and N. Winograd, J. Chem. Phys., 67, 3500 (1977).

8. P. E. Larson, J. of Electron Spectr. and Rel. Phen., 4, 213 (1974).

9. K. S. Kim and N. Winograd, Chem. Phys. Lett., 30, 91 (1975).

1040A

Table 1

Results of Copper Auger Parameter
Determination for Copper Oxide Standards and
Catalyst Samples Analyzed by XPS

Sample	$Cu2p_{3/2}$(ev)[1]	Cu(LMM)(eV)[2]	α'(ev)
Clean Cu	932.1	334.8	1850.9
Cu_2O	932.1	336.8	1848.9
CuO	933.2	335.6	1851.2
Fresh-Unreduced Catalyst	933.6	336.2	1851.0
Fresh-Reduced Catalyst	931.7	336.2	1849.1
Spent-Active Catalyst	931.9	336.5	1849.0
Spent-Deactivated Catalyst	932.0	336.6	1849.0
	932.0	334.6	1851.0

1 $Cu2p_{3/2}$ energies presented as binding energies.
2 Cu(LMM) energies presented in this study as binding energies for consistency.

1040A

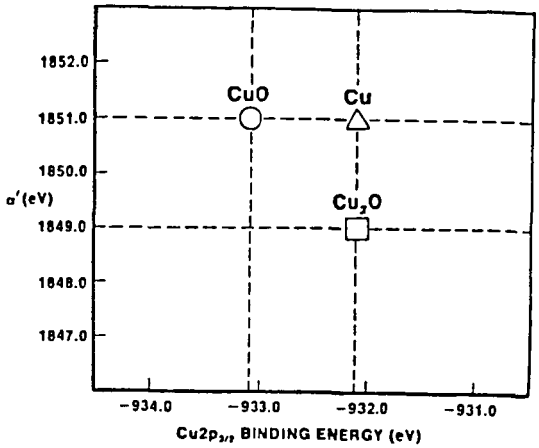

Figure 1: Auger map depicting results of in situ copper oxide study.

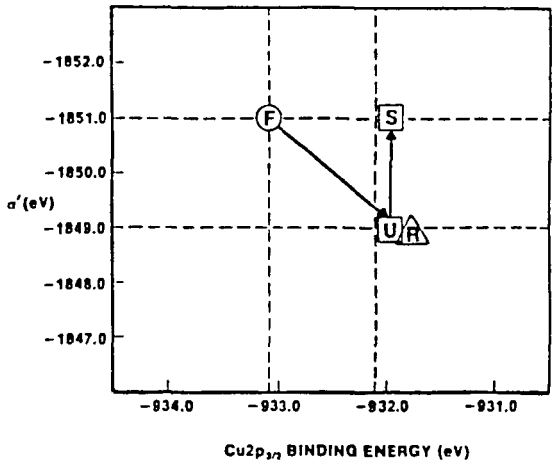

Figure 2: Auger map illustrating the observed changes in the surface copper oxidation state for: (F) fresh-as received catalyst, (R) fresh-reduced catalyst, (U) methanol-active catalyst, and (S) spent catalyst.

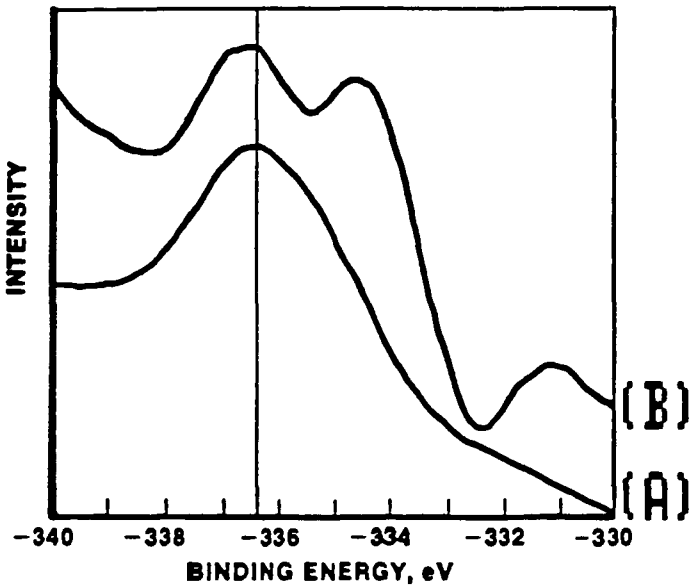

Figure 3: Cu(LMM) X-ray induced Auger spectra for (A) fresh, methanol-active catalyst and (B) spent catalyst.

RELATIONSHIP BETWEEN SURFACE STABILIZED Cu^+ IN COPPER-CHROMIA CATALYSTS AND ACTIVITY FOR METHANOL FORMATION.

G. Apai, J. R. Monnier, M. J. Hanrahan, Research Laboratories, Eastman Kodak, Rochester, New York 14650.

Recent evidence suggests that in Cu-ZnO, the Cu^+ species may be the component responsible for methanol formation. Copper-chromium oxide catalysts also have similar selectivity for methanol synthesis under reaction conditions like those used for Cu-ZnO catalysts. X-ray photoelectron spectroscopy and x-ray diffraction studies of the Cu-Cr oxide catalyst indicate that the activity for methanol formation is associated with a crystalline cuprous chromite phase. The concentration of surface Cu^+ species, stable under H_2 reduction or syngas reaction conditions, is correlated with the activity for methanol formation. Bulk stabilization of $CuCrO_2$ (Cu^+) appears to be responsible for the surface stabilized Cu^+ species. The concentration of surface Cu^+ is dependent upon the Cu/Cr ratio, the calcination temperature, and the nature of the catalyst pretreatment. Comparisons will be made between real and model catalysts. In addition the concentration of these Cu^+ sites is independent of CO_2 addition to the synthesis gas feedstream. The associated decrease in catalytic activity is attributed to the non-catalytic, competitive adsorption of CO_2 on sites active for CH_3OH formation. These results for Cu-Cr oxide provide some interesting similarities and differences in comparison to the Cu-ZnO catalyst.

CHEMISORPTION OF CO, CO_2, O_2 AND H_2 ON THE Cu/ZnO METHANOL SYNTHESIS CATALYSTS

By

G. E. Parris
Air Products & Chemicals, Trexlertown, Pennsylvania

and

K. Klier
Department of Chemistry, Lehigh University, Bethlehem, Pennsylvania

INTRODUCTION

Historically the successful catalysts for methanol synthesis from synthesis gas have always utilized zinc oxide. The addition of chromia, Cr_2O_3, or alumina, Al_2O_3 to the zinc oxide based catalysts were found to be beneficial as supports for extending catalyst life and as promoters to enhance the catalytic activity for synthesis of methanol. These catalysts operate at high pressures (>200 atm) and temperatures (573-623 K), however. The addition of copper oxide to these catalysts resulted in much higher methanol synthesis activity at lower pressures (75 atm) and temperatures (523 K) than observed with the pure components only, or with the ZnO/Cr_2O_3 and ZuO/Al_2O_3 catalysts, (1,2). In addition, the method of preparation of copper catalysts was found to be an extremely important factor(3).

These observations implied that the final state of copper in the mixed $Cu/ZnO/M_2O_3$ catalysts critically determined their high activity and selectivity for the production of methanol. The present work was undertaken to determine the chemisorption properties of CO, CO_2, O_2 and H_2 for a series of binary copper-zinc oxide methanol synthesis catalysts and thereby clarify the reason for the observed mutual promotion effect between Cu and ZnO by identifying the nature of the reactive centers in methanol synthesis catalysts based on copper.

EXPERIMENTAL

The Cu/AnO = 0/100-100/0 catalysts were coprecipitated from nitrate solution by Na_2CO_3, calcined and reduced with H_2/N_2 = 2/98 vol according to a procedure previously described in detail (3,4). The adsorption experiments were conducted in a glass high vacuum volumetric adsorption apparatus with a stationary background vacuum of 10^{-4} Pa. The catalysts were reduced on the adsorption system without exposure to air.

The CO and H_2 isotherms were measured at 293 K up to a final pressure of approximately 16 kPa. The weak and strong capacities were determined as follows: (1) run an adsorption isotherm on a reduced and activated sample, (2) evacuate the sample for 10 minutes then run a second isotherm, and (3) this second isotherm corresponds to the weakly adsorbed gas and the difference between the first and second isotherms is the strongly adsorbed gas. Oxygen chemisorption experiments were conducted at 78 K according to the procedure of Zettlemoyer et al (6). Surface area measurements were made using the BET method with argon as adsorbate.

Carbon dioxide isotherms were studied at 523 K and 293 K on pure ZnO and on the Cu/ZnO = 30/70 catalyst sample. For analysis of the gas phase composition in mixed gas CO/CO_2 redox studies a Varian VGA-100 quadrapole gas analyzer was installed on the chemisorption apparatus. The full details of these experiments are reported elsewhere (5).

RESULTS AND DISCUSSION

CO, O_2 and H_2 Chemisorption

The total CO capacities plotted in Figure 1 are seen to increase with increasing copper content in the binary Cu/ZnO catalysts, with maximum coverage obtained for pure copper. While no adsorption of CO was observed on pure ZnO at 293 K, the saturated coverage obtained for CO on copper is Θ = 0.15-0.18 using the range of site densities estimated for copper surfaces. The strong CO fraction however, shows a double humped feature with broad maxima at the Cu/ZnO = 30/70 and 67/33 compositions. In Figure 2 is shown a comparison between the weak CO and irreversible O_2 chemisorption data. It can be seen from the figure that weak CO capacities show good linearity with irreversible O_2 adsorption, has zero intercept and correctly predicts the observed CO capacity on pure copper.

The series of binary Cu/ZnO catalysts studied here may be divided into two groups, Cu/ZnO = 0/100-30/70 and 40/60-67/33 compositions, which are distinguishable by their crystallite sizes and morphological constitutions as reported earlier (7). Also, a substantial portion of copper was found to be X-ray amorphous (8) and scanning transmission electron microscopy analyses showed this amorphous copper to be in the ZnO phase (7). In an attempt to correlate the chemisorption behavior determined here, with the microstructure and distribution of elements reported earlier in the catalyst particles, four models are proposed below to describe the adsorption behavior of oxygen and carbon monoxide. They are as follows:

Model I — Irreversible O_2 and weak and strong CO adsorption occurs on copper crystallites only.

Model II — Irreversible O_2 and weak CO are adsorbed on copper crystallites; strong CO adsorbs on solute copper.

Model III — Irreversible O_2 is adsorbed on copper crystallites and solute copper. Weak and strong CO are on copper crystallites.

Model IV — Irreversible O_2 is adsorbed on copper crystallites and solute copper. Weak CO on copper crystallites, strong CO on solute copper.

It is apparent from Figure 2 that the sites for weak CO and irreversible O_2 are the same and can readily be attributed to the crystalline copper phase. Further, the strong CO capacities cannot be correlated directly with irreversible O_2 capacities and Models I, III and IV are therefore discarded. On this basis, using the specific adsorption of O_2 on pure copper as well as the measured total surface areas the copper and zinc oxide surface areas in the composite catalysts were determined and the results are shown in Table 1. The methanol synthesis activity does not correlate with either the ZnO or Cu surface areas in the individual catalysts.

With the zinc oxide surface areas available a test can be made of the dependence of strong CO capacities on the surface concentration of solute copper assuming the surface concentration to be proportional to the bulk concentration reported by Bulko et al (8). The plot of surface coverage by strong CO against the concentration of copper solute shown in Figure 3 has a linear portion for each morphology. Therefore, if the strongly bound CO molecules titrate the surface copper solute sites, then the basal (0001) ZnO planes tend to accomodate more solute copper atoms than the prism (1010) planes, which predominate in the compositional ranges Cu/ZnO = 40/60-67/33 and 0/100-30/70 respectively. Since the basal plane of ZnO is formally electrostatically charged while the prism plane is not, its higher accomodation of copper is consistent with the idea that the solute copper species are also charged. These solute copper sites are therefore considered to be the active centers for strong carbon monoxide adsorption and the adsorption characteristics of CO and O_2 are adequately described by Model II.

The amounts of weakly adsorbed hydrogen is proportional to that of irreversibly adsorbed O_2 but the relationship is not linear. Further, the weak H_2 capacities lie above the capacities predicted by pure copper metal and cannot be accounted for by total H_2 coverage on metallic copper surface. Without further evidence therefore, adsorption of H_2 on copper solute sites on the ZnO phase, created by the Cu-ZnO interactions, cannot be excluded.

Redox Behavior with CO/CO_2 Mixtures

The studies on the redox behavior of the Cu/ZnO catalysts were done on, and are of particular interest for the Cu/ZnO = 30/70 catalyst since it is the most active one and was used by Chatikavanij (9) in CO_2 kinetic studies.

The CO_2 isotherms at 523K on a freshly reduced (2% H_2 in N_2) show that there is a very strong interaction of this gas with the Cu/ZnO = 30/70 catalyst, this interaction being stronger but apparently less extensive than with pure ZnO. No carbon monoxide was found in the gas phase when pure CO_2 was added. Upon addition of CO at 523 K to a freshly reduced catalyst, however, a build up of CO_2 in the gas phase was detected. The time dependence of the partial pressure of desorbed CO_2 is shown in Figure 4 for pure ZnO as well as Cu/ZnO = 30/70 samples. There was no preexposure to CO_2 in the samples of Figure 4 and the ZnO areas used in all samples were similar. Also, addition of CO_2 to CO-reduced then outgassed samples gave CO in the gas phase, and as Figure 5 shows, irrespective of whether or not CO_2 is initially present on the surface, the amount of CO_2 desorbed upon CO addition depends only upon the mole fraction of CO in the gas phase.

The redox equilibrium can be represented using the defect notation of Kofstad (12) by the equation

$$CO_{2(g)} + V_o \overset{Kg}{\rightleftharpoons} CO_{(g)} + O_o \qquad 1)$$

where the subscript g denotes gas phase O_o is a lattice oxygen anion and V_o is a lattice oxygen anion vacancy. Adsorption equilibrium for CO and CO_2 on the catalyst surface are given by equations (2) and (3)

$$CO_{2(g)} \overset{K_{CO_2}}{\rightleftharpoons} CO_{2(s)} \qquad 2)$$

$$CO_{(g)} \overset{K_{CO}}{\rightleftharpoons} CO_{(s)} \qquad 3)$$

where subscript s denotes surface.

Using equations (1)-(3) a model equation was developed (5) for the redox equilibria data shown in Figure 5. It was estimated from fitting the data that

$$\frac{K_{CO}}{K_{CO_2}} = 1.3$$

and

$$Kg = 40$$

The value obtained for Kg is neither that for the redox equilibrium of pure ZnO nor pure Cu_2O. This result points to the presence of a compound of intermediate composition such as might be realized from a disolution of copper in zinc oxide as proposed earlier (4). Klier et al (10), in a quantitative study of the kinetics of methanol synthesis for the Cu/ZnO = 30/70 catalyst in the presence of CO_2, reported three sets of constants with which best fits were obtained for three cases involving competitive adsorption schemes of CO, CO_2 and H_2. The values given above for Kg and K_{CO}/K_{CO_2} are consistent with the values they report for the scheme wherein CO_2 competes with both CO and H_2, but CO and H_2 are adsorbed on different sites.

The solubility limit of copper (II) oxide in zinc oxide is 4-6% (11,12) whereas Bulko et al (8) measured up to 16.8%. Since it was earlier concluded that the copper solute species is a charged entity it appears substantiated that the solute copper species exist as copper (I) in zinc oxide.

CONCLUSIONS

The following important conclusions emerge from this work:

1. The sites for weak CO and irreversible O_2 adsorption are the same and readily attributable to the crystalline copper phase.
2. The methanol synthesis activity does not correlate with either the ZnO or Cu surface areas in the composite catalysts.
3. Strong CO chemisorption is associated with the surface copper solute sites which are preferentially accommodated on the electrostatically charged basal plane of ZnO.
4. The ZnO phase in the composite catalyst undergoes redox equilibria in CO/CO_2 mixtures at 523 K with an equilibrium constant that is different from those for pure ZnO or Cu_2O.
5. The solute copper species exist as copper (I) in zinc oxide and are probably the reactive centers in methanol synthesis from synthesis gas.

LITERATURE CITED

(1) M. Patart, French Patent 540,343 (August, 1921).
(2) Brocker, F. J., German Patent 2,116,949 (October 19, 1972); assigned to BASF.
(3) Audibert, Q, and Raineau, A., Ind. Eng. Chem., 20, 1105 (1928).
(4) Herman, R. G., Klier, K., Simmons, G. W., Finn, B. P., Bulko, J. B., and Katylinski, T. P., J. Catal., 56, 407 (1979).
(5) Parris, G. E., Ph.D. Thesis, Lehigh University, Bethlehem, Pa. (1982).
(6) Zettlemoyer, A. C., Yu, Y. F., Chessick, J. J. and Healey, F. H., J. Phys. Chem., 61, 1319 (1957).
(7) Mehta, S., Simmons, G. W., Herman, R. G. and Klier, K., J. Catal., 57, 339 (1979).
(8) Bulko, J. B., Herman, R. G., Simmons, G. W., and Klier, K., J. Phys. Chem., 83, 3118 (1979).
(9) Chatikavanij, V., M. S. Thesis, Lehigh University, 1980.
(10) Klier, K., Chatikavanij, V., Herman, R. G. and Simmons, G. W., J. Catal., 74, 343 (1982).
(11) Chapple, F. H. and Stowe, F. S., Proc. Brit. Ceram. Soc., 1, 45 (1964).
(12) Schiavello, M., Pepe, F. and DeRossi, S., J. Phys. Chem., 92, 109 (1974).

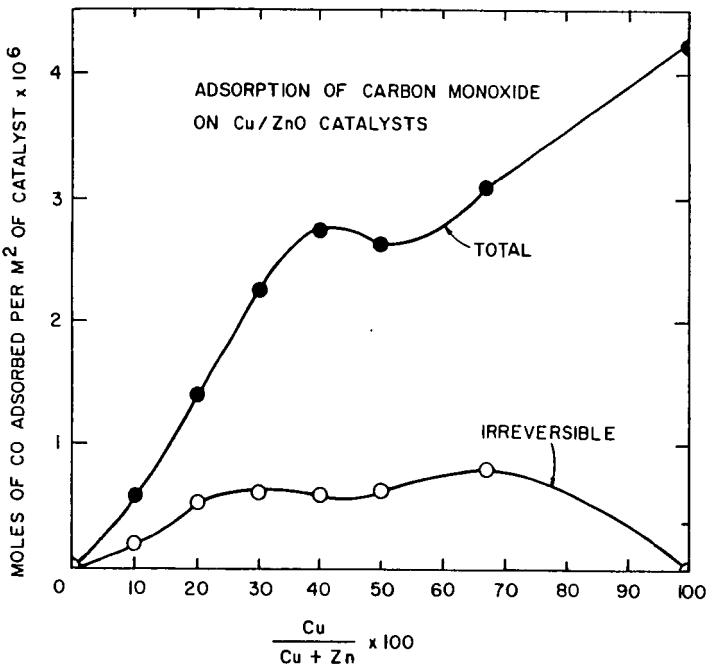

Figure 1. The dependence of the carbon monoxide saturation adsorption (total) and irreversible adsorption (irreversible) on the Cu/ZnO ratio in the binary copper-zinc oxide catalysts.

Table 1

Surface Area of Copper Metal and Zinc Oxide in the Binary Cu/ZnO Catalysts

Catalyst Composition Cu/ZnO	Cu Surface Area m^2/g Catalyst	ZnO Surface Area m^2/g Catalyst	Total Surface Area m^2/g Catalyst
0/100	--	24.1	24.1
10/90	4.9	30.1	35.0
20/80	8.9	27.6	36.5
30/70	16.0	23.3	39.3
40/60	6.5	8.5	15.0
50/50	5.7	5.4	11.1
67/33	3.9	3.5	7.4
100/0	0.62	--	0.62

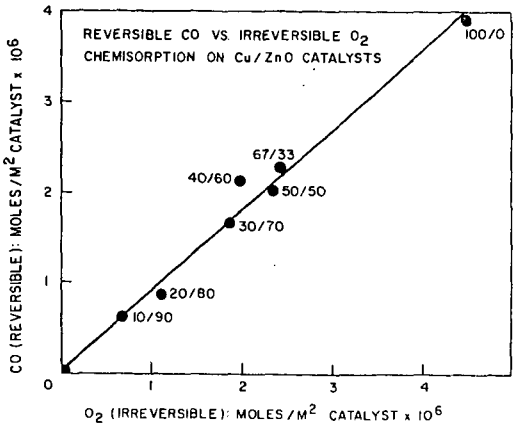

Figure 2. The relation between the amounts of weakly chemisorbed carbon monoxide and irreversibly chemisorbed oxygen indicating that these two adsorbates are a measure of copper metal surface area.

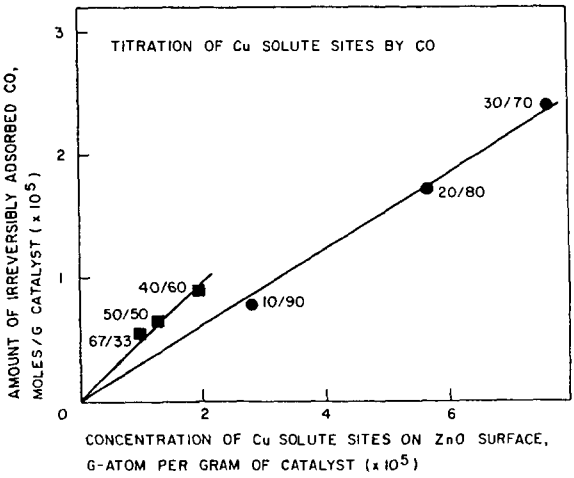

Figure 3. The dependence of the amount of irreversibly chemisorbed carbon monoxide on the concentration of amorphous copper found by X-ray diffraction and by STEM. The (1010) prism planes of zinc oxide are exposed in the Cu/ZnO = 10/90, 20/80, and 30/70 catalysts and the (0001) basal planes of ZnO are exposed in the Cu/ZnO = 40/60, 50/50, and 67/33 catalysts.

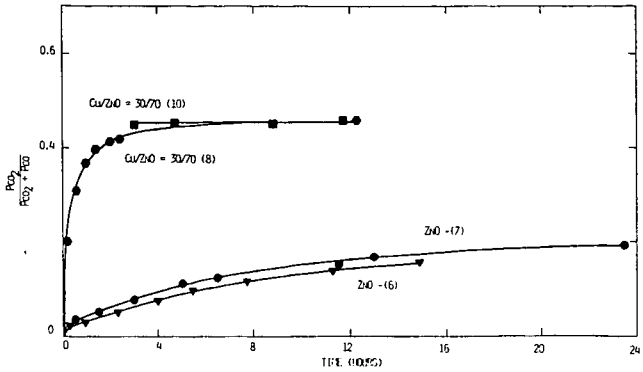

Figure 4. The time dependence of CO_2 partial pressure over ZnO and Cu/ZnO catalysts after CO is admitted to catalyst prereduced in H_2/N_2 = 2/98 vol. % at 523K.

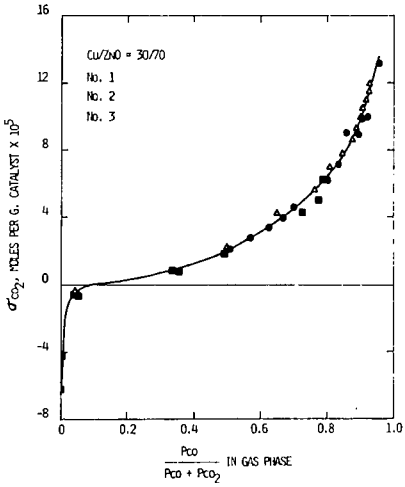

Figure 5. The dependence of σ_{CO_2}, defined as the cummulative amount of CO_2 desorbed from the catalyst surface less the initial amount of CO_2 adsorbed prior to the addition of CO, on the mole fraction of CO in the gas phase.

Nature of H_2 Adsorption Sites in Cu/ZnO Synthesis Catalysts

D. L. Roberts and G. L. Griffin

Department of Chemical Engineering and Materials Science
University of Minnesota, Minneapolis, MN 55455

Abstract

For a co-precipitated Cu/ZnO mixture that is representative of methanol synthesis catalysts, we observe that H_2 adsorption occurs at isolated Cu sites on the catalyst surface. These H_2 adsorption sites differ from those previously observed on pure ZnO samples in two respects: The range of H_2 desorption energies is significantly higher (21-30 kcal/mole for the 10:90 Cu:ZnO mixture, vs. 16-21 kcal/mole for pure ZnO), and the pretreatment temperature needed to activate the sites is lower (523 K for the Cu/ZnO mixture, vs. 673 K for pure ZnO). This suggests that the enhanced activity of Cu/ZnO catalysts, relative to ZnO catalysts, is due to Cu sites that adsorb H_2 more strongly and which maintain their activity at lower temperatures.

Introduction

Catalysts for the direct synthesis of alcohols from $CO:H_2$ mixtures must satisfy two functional requirements. They must activate the CO molecule for reduction without directly dissociating the C-O bond, and they must activate the H_2 molecule to perform the reduction. These two functions are combined quite effectively in the Cu/ZnO catalysts for methanol synthesis (1,2), which hydrogenate CO to CH_3OH with better than 99% selectivity (3).

Understanding the hydrogenation mechanism on these ZnO-based catalysts is important, not only for selecting the optimum operating conditions for methanol catalysts but also for designing catalysts to perform higher alcohol synthesis or other hydrogenation reactions. As a prerequisite for understanding the hydrogenation mechanism itself, in this paper we discuss our current knowledge of the H_2 adsorption sites on ZnO and Cu/ZnO mixtures.

H_2 Adsorption on ZnO

The distinguishing feature of H_2 adsorption on oxide catalysts is that adsorption occurs *via* heterolytic dissociation of the H_2 molecule at polar surface sites consisting of co-ordinatively unsaturated cation-anion pairs. On ZnO, this adsorption process has been conclusively shown to occur at so-called Type I sites (4-7):

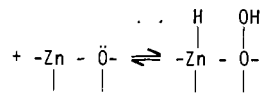

1)

Reaction 1 is demonstrated by bands in the IR spectrum of H_2-saturated catalysts at 1710 cm-1 and 3490 cm-1, assigned to Zn-H and O-H stretching vibrations respectively (4-7).

The energetics of the Type I adsorption sites are fairly complex. Adsorption is activated but reversible at room temperature. A range of adsorption and desorption energies are observed, suggesting that more than one kind of Type I site exists. The equilibrium adsorption energy is 12-13 kcal/mole, the activation barrier for adsorption is 3-8 kcal/mole, and the desorption energy is 16-21 kcal/mole (7).

A second type of H_2 adsorption state has also been identified that is irreversible at room temperature (5). This so-called Type II state is not IR active, and consequently has not been studied as intensively as the Type I state. Dent et al. (8) have shown that Type II hydrogen is not involved in hydrogenation reactions, at least for the case of ethylene hydrogenation. The authors go on to speculate that Type II hydrogen may be bound in sub-surface sites, and therefore is non-reactive. While this remains to be proven conclusively, we will restrict the remaining discussion to Type I sites.

The geometry of the Type I sites has been partially determined. Temperature programmed desorption experiments show that H_2 molecules are adsorbed at spatially discrete sites: The coverage dependence of the TPD spectra indicate that desorption obeys first-order kinetics (cf. Fig. 1 below). Also, co-adsorbed H_2-D_2 mixtures retain most of their isotopic identity when desorbed. Both results are in marked contrast to the second order desorption kinetics and isotopic scrambling seen in TPD spectra of H_2 and D_2 on metals, where H atoms may interact with any of several neighbors during desorption.

The Type I sites are located within next-nearest neighbor proximity of each other. This is shown by the shifts of the ZnH and OH vibrational frequencies that occur as H_2 coverage increases. These shifts can be explained on the basis of electrodynamic and inductive interactions between oscillating ZnH and OH dipoles, provided that H_2 molecules adsorbed at different sites are within two lattice spacings of each other (9). (The shifts do not appear to be caused by long range electronic interactions involving the ZnO conduction band electrons, because the background transmission of the sample, and hence the Fermi level, remains unchanged during H_2 adsorption). Further evidence that the sites are spatially proximate is given by the observation that scrambling of H_2-D_2 mixtures does occur readily over ZnO at room temperature, where adsorption is reversible (5). This shows that migration and exchange between Type I sites does occur, albeit with a modest activation barrier.

Additional information about the nearest-neighbor geometry of the sites is provided by spectroscopic measurements of co-adsorbed CO:H_2 mixtures (10,11). These results show that the ZnH vibrational band undergoes two sequential, discrete frequency shifts as the CO coverage is increased. In contrast, the OH vibration shows only a continuous frequency shift with increasing CO coverage. Thus the Zn cation of the Type I sites appears to have two nearest neighbor sites that can adsorb CO, while the O anion of the Type I site has no such neighbors. Since the CO adsorption state that is occupied under the conditions of these experiments is known to occur at coordinately unsaturated Zn cations (12), this leads to the perhaps surprising conclusion that the Zn cation of the Type I site has two unsaturated Zn cations as neighbors, while the O anion has no unsaturated cations as neighbors (other

than its own Type I cation partner). However, such a "triad" of unsaturated Zn cations would be expected at an $O^{=}$ vacancy produced when a three-fold co-ordinated surface O anion is removed from the surface layer (10). Moreover, if this anion vacancy is produced by a dehydration reaction with the proton of a neighboring surface OH group, then the unsaturated O anion that remains after proton removal can serve as the anion partner in the Type I site.

Such oxygen vacancies can be most easily imaged on the basal $(000\bar{1})$ oxygen plane (10). This is supported by the fact that Type I sites are most easily observed on powdered samples that contain a large fraction of polar planes in their crystal morphology (13), and also by the fact that sublimation occurs more readily on the basal oxygen face (14). However, recent studies of ZnO single crystal surfaces have raised the possibility that such vacancies might also be produced at step defects on the $(10\bar{1}0)$ prism planes (15,16).

One other important feature of the Type I sites is their strong poisoning by adsorbed H_2O or CH_3OH (5):

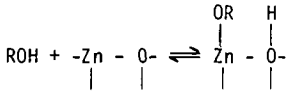

2)

Reaction 2 is irreversible at room temperature, indicating that the desorption energy of these adsorbates is much greater than for H_2. Quantitative measurements of the desorption energies are still needed.

It is generally believed that the activation mechanism for producing the Type I site is dehydration to produce a cation-anion pair site. While this is certainly a necessary condition, experience in our laboratory has shown that it is not sufficient. Heating ZnO samples to less than 673K produces highly dehydrated surfaces, as indicated both by a sharp decrease in the IR bands due to residual OH species on the sample, and by the ability of the sample to re-adsorb H_2O. However, these surfaces are <u>not</u> active for the adsorption of H_2. In light of the discussion above, this suggests that an additional requirement for activating the Type I sites is that the dehydration step must also produce an $O^{=}$ anion vacancy. Adsorption of H_2O or CH_3OH thus represents a strong poisoning reaction, because these species re-occupy the $O^{=}$ vacancy.

H_2 Adsorption on Cu/ZnO

The results discussed above have been obtained for pure ZnO. While the ZnO Type I sites have been suggested as the source of the hydrogenation activity in Cu/ZnO synthesis catalysts (3), their presence has not been conclusively demonstrated on Cu/ZnO mixtures. As a first test for their presence, we therefore examined the H_2 adsorption behavior of a Cu/ZnO mixture with a 10:90 Cu:Zn ratio, prepared using the co-precipitation technique described by Hermann et al. (3).

In figures 1 and 2 we compare the H_2 desorption spectra of pure ZnO and the Cu/ZnO mixture. After outgassing each sample at the necessary temperature, the spectra were obtained by admitting the indicated pressure

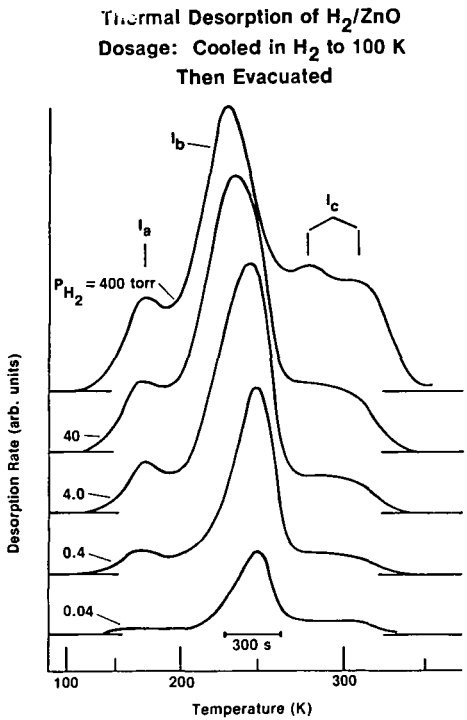

FIGURE 1

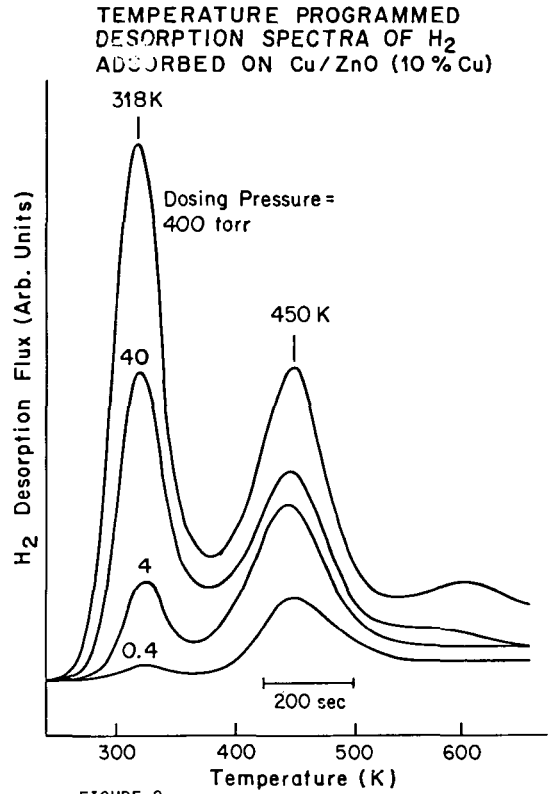

FIGURE 2

of H_2 to the sample cell at room temperature, cooling the sample to 100K, evacuating the non-adsorbed gas, and then warming the sample (heating rate = 1.5 K/sec) while monitoring the flux of desorbing H_2. This dosing procedure was required to overcome the activation barrier for adsorption noted above.

The results for pure ZnO (Figure 1) have been discussed elsewhere in more detail (7). First we note that the spectra are quite complex, suggesting the presence of multiple binding states. The amount of H_2 adsorbed increases with dosing pressure, indicating that the activation barrier for adsorption increases with coverage. The peak temperatures are only weakly dependent on coverage, indicating first order kinetics. (First order kinetics are also indicated by the absence of isotopic scrambling, as noted above). The peak temperatures occur at 170, 240, 270, and 310 K, corresponding to desorption energies of 12, 16, 18, and 21 kcal/mole, respectively. No additional information about the individual states corresponding to each peak is available, except that the state at 170 K has a unique OH vibrational frequency and a small enough desorption energy that it is not occupied at room temperature. Finally, we note that it is necessary to outgas the sample at 673 K or above in order to observe any of these H_2 adsorption states.

The spectra for the Cu/ZnO samples are shown in Fig. 2. As was the case with pure ZnO, we see that the amount adsorbed increases with dosing pressure, indicating that adsorption is an activated process and that the activation barrier increases with coverage. The peak temperatures are again independent of H_2 coverage, suggesting first order desorption kinetics. However, two differences from the results for ZnO are observed: The peak temperatures are 310 K and 450 K, corresponding to desorption energies of 21 and 30 kcal/mole. These are higher than the range of energies found for ZnO. In addition, these experiments were performed using samples outgassed at 523 K, instead of the 673 K needed for ZnO. As mentioned above, pretreating ZnO at the lower temperature results in a surface with negligible H_2 adsorption capacity.

Discussion

We first consider what these results indicate about chemical bonding at the adsorption sites on Cu/ZnO catalysts. The fact that H_2 adsorption is observed after pretreatment at much lower temperature for the Cu/ZnO mixture than for pure ZnO indicates either that Cu species make it easier for the Type I ZnO sites to be activated, or else that Cu species themselves can function as the cations in Type I sites that have a much lower activation temperature. Competitive adsorption experiments with $CO:H_2$ mixtures described elsewhere (17) indicate that the latter explanation is correct; that is, the Cu species themselves participate as the cations in Type I sites analogous to those found on pure ZnO. The lower temperature required to activate the Cu sites suggests that the $O^=$ vacancy needed at a Type I site is more easily produced at a Cu neighbor, which is consistent with the lower enthalpy of decomposition of bulk CuO (36 kcal/mole for CuO, vs. 81 kcal/mole for ZnO (18)).

The higher desorption energy for H_2 may be the result of the d-electron vacancy on a divalent Cu cation, which would stabilize the CuH hydride bond (19).

Finally, we consider the implication of these results for the hydrogenation

mechanism on Cu/ZnO catalysts. The lower pretreatment temperature needed to activate the Cu Type I sites is remarkably consistent with the lower operating temperature required for Cu/ZnO synthesis catalysts, relative to the high pressure ZnO catalysts. The stronger H_2 adsorption energy may also contribute to the improved activity of the Cu/ZnO catalysts, although more detailed knowledge of the energetics of the subsequent reaction steps is needed before this conclusion can be stated with certainty. Finally, it is interesting to note that this H_2 adsorption behavior has not been reported for Cu species prepared on other supports. This suggests that the basicity and/or the tetrahedral coordination geometry of the ZnO lattice may be necessary to generate Type I cation-anion sites. This last point suggests that the potential of ZnO as a support material for hydrogenation catalysts should be more fully explored.

Acknowledgment: One of us (DLR) acknowledges fellowship support from Chevron Research Company, Standard Oil Company of California. This research was supported by the National Science Foundation, grant no. CPE-8105823.

References

1) G. Natta; in Catalysis (P. H. Emmett, ed., Reinhold, 1955) Vol. 3, p. 349

2) K. Klier; Adv. in Catal. 31 243 (1982)

3) R. G. Herman, K. Klier, G. W. Simmons, B. P. Finn, J. B. Bulko, and T. P. Kobylinski; J. Catal. 56 407 (1979)

4) R. P. Eischens, W. A. Pliskin, and M. J. D. Low; J. Catal. 1 180 (1962)

5) R. J. Kokes, A. L. Dent, C. C. Chang, and L. T. Dixon; JACS 94 4429 (1972)

6) F. Boccuzzi, E. Borello, A. Zecchina, A. Bossi, and M. Camia; J. Catal. 51 150 (1978)

7) G. L. Griffin and J. T. Yates, Jr.; J. Catal. 73 396 (1982)

8) A. L. Dent and R. J. Kokes; J. Phys. Chem. 73 3781 (1969)

9) G. L. Griffin and J. T. Yates, Jr.; J. Chem. Phys. 7 3744 (1982)

10) F. Boccuzzi, E. Garrone, A. Zecchina, A. Bossi, and M. Camia; J. Catal. 51 160 (1978)

11) G. L. Griffin and J. T. Yates, Jr.; J. Chem. Phys. 77 3751 (1982)

12) R. R. Gay, M. H. Nodine, V. E. Henrich, H. J. Zeiger, and E. I. Solomon; JACS 102 6752 (1980)

13) M. Grunze, W. Hirschwald, and D. Hofmann; J. Crystal Growth 52 241 (1981)

14) D. Kohl, M. Henzler, and G. Heiland; Surf. Sci. 41 403 (1974)

15) W. H. Cheng, S. Akhter, and H. H. Kung; J. Catal. 82 341 (1983)

16) L. Chan and G. L. Griffin (to be submitted)

17) Handbook of Chemistry and Physics (52nd ed., Chem. Rubber Co., Cleveland, 1972) Table D-61

18) B. Kunz; in Theory of Chemisorption (Topics in Current Physics, Vol. 19, Springer Verlag, 1980) p. 115

MICROSTRUCTURE OF $Cu/ZnO/Al_2O_3$ METHANOL SYNTHESIS CATALYSTS STUDIED BY SCANNING AND TRANSMISSION ELECTRON MICROSCOPY AND DIFFRACTION METHODS

P. B. Himelfarb, G. W. Simmons, and K. Klier

Department of Metallurgy and Materials Engineering,
Department of Chemistry, and Center for Surface and
Coatings Research, Lehigh University,
Bethlehem, PA 18015

INTRODUCTION

Catalysts containing Cu/Zn/Al are well known active catalysts in methanol synthesis and the water-gas shift reaction, and have been described extensively in the literature (1-6). However, limited information is available on the elemental distributions in the various morphologies present in the many preparative variants of these catalysts. The understanding of these material properties and their relationship to synthesis activity is a primary goal in catalyst characterization. In the present work, transmission electron microscopy coupled with diffraction and elemental analysis was used to compare the chemical structure, morphology and elemental distribution in three different preparations of active Cu/Zn/Al catalysts.

EXPERIMENTAL

Two catalysts were prepared from Zn(II), Cu(II) and Al(III) acetate solution by coprecipitation with sodium carbonate at 90°C until a pH of 6.9 was reached to produce the compositions, Cu/Zn/Al equal to 54.4/24.3/23.3 and 27.3/63.6/9.0 at.% (prepared at Lehigh University). Another catalyst was similarly prepared from nitrate solution at 30°C to produce Cu/Zn/Al equal to 60.0/30.0/10.0 at.% (prepared at the University of Virginia). In all preparations, the precipitates were washed extensively, calcined in air at 350°C, and reduced at 250°C in a 60-70 cc/min 2% H_2/N_2 mixture for the time required for the stoichiometric reduction of CuO to Cu. Methanol synthesis activities were determined in a tubular fixed bed flow reactor equipped with pressure, temperature and flow rate controls (7,8). Methanol yields were determined by gas chromatography.

A Philips EM 400T transmission electron microscope (TEM) which included a scanning transmission mode (STEM) was used in the characterization studies. Samples were prepared by dispersing the catalyst powders in ethanol and placing a drop of the dispersion on a carbon coated titanium grid. Exposure time to air was minimized by preparing and transporting specimens in a N_2 filled glove bag. Energy dispersive X-ray analysis (EDS) for elemental identification and quantification was obtained in the manner described in references (4) and (9).

RESULTS

Methanol yields and respective surface areas for the catalysts studied are given in Table I. Data published for catalysts of similar

TABLE I

ACTIVITIES OF Cu/Zn/Al CATALYSTS

#	Catalyst Cu/Zn/Al at.%	Surface Area m^2/g	MeOH Yield g/g cat/hr
1	60.0/30.0/10.0[a]	54.2	1.35
2	52.4/24.3/23.3[b]	26.0	1.37
3	27.3/63.6/9.0[c]	61.8	1.55
4	67.0/33.0/0.0 (7)	7.4	0.41
5	30.0/70.0/0.0 (7)	39.3	1.35

[a]Prepared from nitrate solution, tested at 80 atm, 255°C, GHSV = 5600 hr^{-1}, $H_2/CO/CO_2$ = 69/27/4 (8).

[b]Prepared from acetate solution, tested at 75 atm, 250°C, GHSV = 5000 hr^{-1}, $H_2/CO/CO_2$ = 70/24/6 (10).

[c]Prepared from acetate solution, tested at 75 atm, 250°C, GHSV = 3750 hr^{-1}, $H_2/CO/CO_2$ = 70/24/6.

Cu/Zn compositions prepared without Al are given for comparison (7). As shown, high yields are maintained within a large variation in elemental composition. Elemental distribution, morphology, and chemical structure were determined for catalysts 1 and 3 (cf. Table I), and the results were compared with previously published data on catalyst 2 (10).

Two distinctly different morphologies were observed in both catalysts 1 and 3. One morphology was a platelet structure containing all three metals (Cu/Zn/Al) which gave a ZnO (0001) electron diffraction pattern, and appeared similar to the platelet morphology reported in catalyst 2 (10). The other morphology was lacelike and contained two metals (Cu/Zn) in the form of Cu and ZnO as determined by selected area diffraction (SAD). The lace-like morphology appeared similar to that found in an active Cu/ZnO (30/70 at.%) methanol catalyst (4,11). Micrographs of the ternary platelet and binary lace-like morphologies with corresponding dark field images from ZnO are given in Figures 1 and 2, respectively. The dark field micrographs show that the ZnO is more highly dispersed in the ternary platelet morphology. An SAD pattern of a platelet is given in Figure 3 which shows that the ZnO (0001) and Cu($\bar{1}$11) planes are parallel to the surface of the platelet. The epitaxial relationship between the Cu and ZnO shows that the Cu[0$\bar{2}$2] axis is parallel to the ZnO[1$\bar{2}$10] axis, which was similarly found in catalyst 2 (10) and in the Cu/ZnO (30/70 at.%) catalyst (4). Although the spot patterns appear to have been produced by single crystals, they originate from highly dispersed Cu and ZnO crystallites in crystallographic registry.

Crystal sizes of ZnO determined from TEM dark field images in the ternary platelet and binary lace-like morphologies, and Cu and ZnO crystallite sizes determined by X-ray diffraction line broadening are given in Table II for catalysts 1 and 3. Published data for catalyst 2 is also given for comparison (10). The microstructural similarities

TABLE II

MORPHOLOGIES AND CRYSTALLITE SIZES OF Cu/Zn/Al CATALYSTS

Catalyst #	Bulk Composition Cu/Zn/Al at.%	Abundance[a] of Platelets	ZnO by TEM (nm)[b]		XRD (nm)[c]	
			Platelet	Binary	ZnO	Cu
1	60.0/30.0/10.0	≅ 10%	2.6	9.1	7.0	12.4
2	52.4/24.3/23.3	≅100%	2-4	d	--	--
3	27.3/63.6/9.0	≅ 20%	2.6	11.9	12.3	8.9

[a]Given as the percent abundance of the ternary platelet morphology compared to the binary lace-like morphology.

[b]ZnO crystal sizes are an average of 100 measurements from TEM dark field measurements produced from the ZnO{10$\bar{1}$0}, {0002}, and {10$\bar{1}$1} reflections for the binary morphology, and from the ZnO(1$\bar{1}$00) diffraction spot for the platelet morphology.

[c]Crystallite sizes determined by X-ray diffraction line broadening using the Scherrer equation corrected for instrumental broadening (12); the Cu{111} and an average from the ZnO{10$\bar{1}$0}, {0002}, and {10$\bar{1}$1} reflections were used.

[d]Lace-like binary phase not present.

are striking in the platelet morphology in that the ZnO crystal sizes are essentially identical in catalysts 1, 2 and 3, and the epitaxial relation between Cu and ZnO was commonly observed. The higher average ZnO crystal sizes, determined by X-ray diffraction, reflect the higher concentration of the binary lace-like morphology which has larger ZnO crystallite sizes than the platelet morphology. In contrast to catalysts 1 and 3, catalyst 2 had large (greater than 0.1 μm) Cu particles and the binary lace-like morphology was not detected (10).

Elemental distributions in the platelets determined by EDS were: Catalyst 1 had the composition 4.5 ± 3.8 at.% Cu, 75.5 ± 2.8 at.% Zn, and 20.0 ± 1.9 at.% Al from 27 measurements, and catalyst 3 platelets contained 24.5 ± 7.9 at.% Cu, 56.6 ± 5.8 at.% Zn, and 18.9 ± 7.8 at.% Al from 23 measurements. No Al was detected in the binary lace-like morphology in catalyst 3, and in catalyst 1 a weak Al peak was sometimes observed which corresponded to less than 1 wt.% in the binary morphology. No evidence of crystalline Al-containing compounds was found by either X-ray or electron diffraction analysis. EDS analysis of platelets in catalyst 2 resulted in 8 ± 2 at.% Cu, 50 ± 5 at.% Zn, and 42 ± 4 at.% Al (10).

DISCUSSION

Comparison of the methanol yields for the three Al-containing catalysts studied shows that active catalysts can be prepared from either acetate or nitrate solutions, and that high concentrations of

Cu are not necessary for high activity.

The activity of catalyst 2 has been attributed to the platelet morphology because the only other morphology present was large inactive Cu particles, as reported earlier (10). Since methanol yields for catalysts 1, 2 and 3 are similar, and the relative abundance of the platelet and lace-like morphologies varied significantly (see Table II), the activity of the platelet and lace-like morphologies must be comparable. Binary Cu/ZnO catalysts have been prepared with high methanol synthesis activity (see catalyst 5 in Table I). The activity of the binary lace-like morphology in catalysts 1 and 3, which contains little or no Al, supports the view that an Al_2O_3 component serves basically as a structural promoter (2).

A comparison of catalysts 2 and 3 (which have similar activities but dramatically different Cu/Zn ratios) to catalysts of similar Cu/Zn ratios prepared without Al (see catalysts 4 and 5 in Table I) shows that the addition of Al widens the Cu/Zn compositional range which can be used to produce an active catalyst. This is a result of the increased dispersion of Cu and ZnO occurring in the Al-containing catalysts.

In summary, active Cu/Zn/Al methanol synthesis catalysts do not require high concentrations of copper. Three basic morphologies — large Cu particles (greater than 0.1 μm), Cu/Zn/Al polycrystalline platelets, and a binary Cu/ZnO morphology can be produced in different amounts by variations in the initial elemental concentrations and preparation conditions. The ternary platelet and binary lace-like morphologies are active in methanol synthesis, which is believed to be a result of the intimate dispersion of the Cu and ZnO crystallites in both morphologies. The Al component, which appears amorphous, is a structural support in the platelets, and widens the Cu/Zn ratio range for which high dispersion of Cu and ZnO can be obtained.

ACKNOWLEDGMENTS

This research was supported by the U.S. Department of Energy through the Pittsburgh Energy Technology Center (Grant No. DE-FG22-80PC30265).

REFERENCES

(1) Kung, H. H., Catal. Rev. - Sci. Eng. 22(2), 235 (1980).

(2) Klier, K., Adv. Cat. 31, 243 (1982).

(3) Shimomura, K., Ogawa, K., Oba, M, Kotera, Y., J. Catal. 52, 191 (1978).

(4) Mehta, S., Simmons, G. W., Klier, K., Herman, R. G., J. Catal. 57, 339 (1979).

(5) Natta, G., (Emmett, P. H., ed.) "Catalysis Volume III," Reinhold Publishing Corp., New York, 1955, p.349.

(6) Imperial Chemical Industries, "Catalyst Handbook," Springer-Verlag, New York, Billing and Sons Ltd., 1970.

(7) Herman, R. G., Klier, K., Simmons, G. W., Finn, B. P., Bulko, S. B., J. Catal. 56, 407 (1979).

(8) Bieser Jr., A. L., Ph.D. Thesis, University of Virginia, Charlottesville, VA (1983).

(9) Himelfarb, P. B., Master's Thesis, University of Virginia, Charlottesville, VA (1983).

(10) Herman, R. G., Simmons, G. W., Klier, K., Proceedings of the 7th International Congress on Catalysis, Tokyo, June 30 - July 4, 1980 (1981).

(11) Cullity, B. D., "Elements of X-Ray Diffraction," 2nd edition, Addison-Wesley Publishing Co., Inc. 1978, p.284.

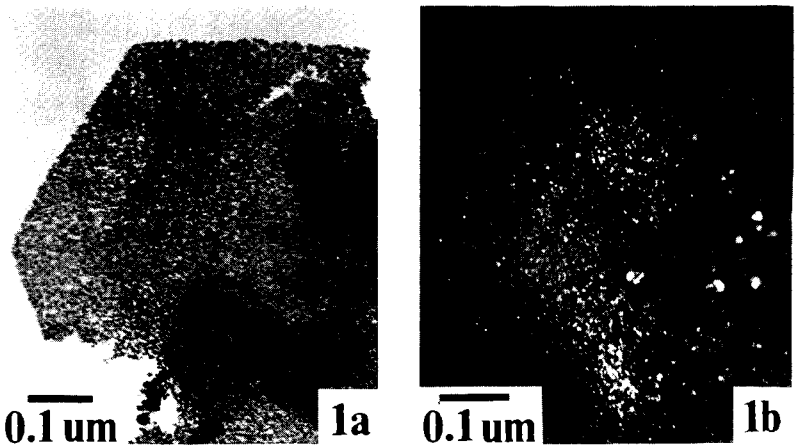

Figure 1. Electron micrographs of ternary platelet morphology in catalyst 3 (Cu/Zn/Al at.% = 27.3/63.6/9.0). (a) Bright field image, (b) dark field image from a ZnO($1\bar{1}00$) diffraction spot (see Fig. 3).

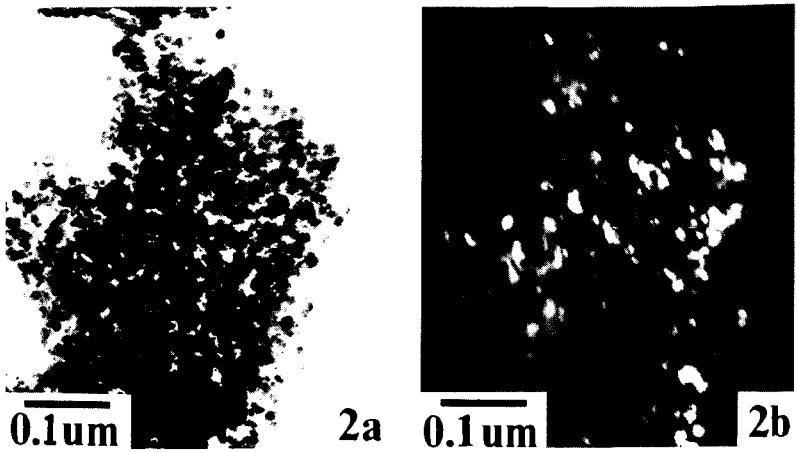

Figure 2. Electron micrograph of binary lace-like morphology in catalyst 3 (Cu/Zn/Al at.% = 27.3/63.6/9.0). (a) Bright field image, (b) dark field image from ZnO{$10\bar{1}0$}, {0002}, and {$10\bar{1}1$} diffraction rings.

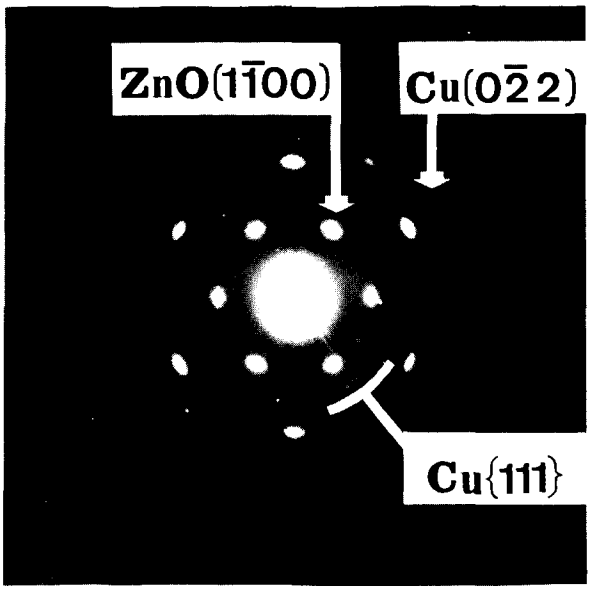

Figure 3. Selected area diffraction pattern of the ternary platelet morphology in catalyst 3 (Cu/Zn/Al at.% = 27.3/63.6/9.0) showing randomly oriented Cu, from the Cu{111} ring pattern, and single crystal patterns of Cu($\bar{1}$11) and ZnO(0001), defined by the Cu(0$\bar{2}$2) and ZnO(1$\bar{1}$00) diffraction spots.